Transworld Research Network
37/661 (2), Fort P.O., Trivandrum-695 023, Kerala, India

Recent Res. Devel. Physics, 4 (2003): 287-307 ISBN: 81-7895-078-2

14 Magnetic properties and magnetotransport in nanoparticle assemblies

D. Kechrakos and K.N. Trohidou
Institute of Materials Science, National Center for Scientific Research "Demokritos"
15310 Athens, Greece

Abstract

We present Monte Carlo simulations of the magnetic properties (hysteresis, temperature dependent magnetization) and the giant magnetoresistance of systems containing magnetic particles (or grains) with diameters in the range of a few nanometers. Granular films with a metallic or insulating matrix, frozen ferrofluids (FF) and thin films containing magnetic nanoparticle aggregates are systems belonging to this class of materials. Emphasis is given to the role of inter-particle interactions, both magnetostatic and exchange, and the modifications they introduce to the magnetic behaviour of nanoparticle assemblies. The giant magnetoresistance of a metallic granular film is calculated implementing Kubo's formula for the electronic conductivity in the Monte Carlo relaxation procedure. The dependence of the magnetoresistance on external parameters (temperature, applied field)

Correspondence/Reprint request: Dr. D. Kechrakos, Institute of Materials Science, National Center for Scientific Research "Demokritos", 15310 Athens, Greece. E-mail : dkehrakos@ims.demokritos.gr

and intrinsic particle properties (grain size and morphology, anisotropy) is demonstrated and compared to experiments. For films containing nanoparticle aggregates, we model the growth mechanism and characterize the final morphology by a fractal dimension. We quantify the relation between the aggregate morphology and their magnetic properties by proving the existence of scaling relations between the magnetic properties of the aggregates and their size.

1. Introduction

Magnetic nanoparticles have been the subject of extensive experimental and theoretical research over the last five decades. Assemblies of fine magnetic particles are formed by nature in many biological and geological systems (human blood, soils, rocks) or are grown synthetically in the laboratory. A strong motive for developing these systems is the basic understanding of their magnetic properties (finite size effects) as well as their attracting technological applications and potentials in the magnetic recording industry [1, 2]. Among the most common synthetic materials containing fine magnetic particles are granular solids that consist of fine magnetic particles of a transition metal (Fe, Ni, Co) or a compound (CoPt) with a diameter of a few nanometers embedded in a non-magnetic matrix (typically SiO_2, BN, Al_2O_3, Cu, etc.). In addition, to granular solids, colloidal dispersions of fine magnetic particles (e.g. Fe_3O_4, γ-Fe_2O_3) known as ferrofluids or magnetic fluids have been extensively studied as regards their magnetic and rheological properties and have found numerous applications in biotechnology and sensor technology [3].

The magnetic properties of fine particles with diameters in the range of a few nanometers stem from their unique feature of consisting of a single magnetic domain. This feature is the outcome of the high energy cost for the formation of a domain wall in their volume and it occurs as long as their size is smaller than the exchange correlation length. In the single-domain regime, the magnetization process of a nanoparticle is realized by rotation of the magnetic moment, instead of domain-wall motion. The magnetization rotation model was introduces and studied theoretically by Stoner and Wolfarth [4] and provides an indispensable tool for the interpretation of the low-temperature hysteresis measurements in dilute samples. At finite temperature, the reversal of magnetization is achieved by thermal activation over the single particle anisotropy barrier that leads to a temperature and time dependence of the magnetization. This effect was first analysed by Néel [5] who expressed the relaxation time for reversal by means of the Arrhenius-Néel law $\tau = f_0 \exp(-\Delta E/k_B T)$, where ΔE is the anisotropy energy barrier and $f_0 \sim 10^9\ s^{-1}$ is the attempt frequency. Bean and Livingston [6] assumed further that the criterion for thermal stability of a magnetic nanoparticle against thermal fluctuations is the value of the ratio of the relaxation time to the measuring time (t_m) which is characteristic of the experimental probe used (Mössbauer, etc). Thermal stability is lost when $\tau = t_m$, which for most experimental probes corresponds to $\tau \sim 100$ s and consequently, to a characteristic temperature $T_b \sim 25(\Delta E/k_B)$ called blocking temperature. For temperatures $T > T_b$, the ensemble of single-domain particles behaves as a gas of paramagnetic molecules with giant magnetic moment ($m \sim 10^3 \mu_B$) and the corresponding equilibrium state is known as superparamagnetism [6]. The conceptual framework composed by the models of Stoner-Wolfarth and Néel is an invaluable theoretical tool for the interpretation and prediction of the temporal and thermal

evolution of the magnetic properties of isolated nanoparticles or dilute assemblies. Indeed, the exploitation of this theory in the determination of the particle size distribution has been the subject of intensive experimental and theoretical work over the last years [7, 8]

In an assembly of magnetic nanoparticles, especially at high densities, interparticle interactions have an important and sometimes dominant role in the formation of the magnetic behavior. Magnetostatic interactions between the particles are always present owing to the magnetic moment each particle carries. Due to their long range character they cannot be neglected except at the extreme dilute limit. Furthermore, exchange interaction between the particles appears when there is physical contact between them, due to the overlap of the wavefunctions of the surface atoms. The exchange interaction is expected to play an important role in samples with concentration close and above the percolation threshold. Finally, a metallic matrix can mediate an indirect exchange interaction (RKKY) between the nanoparticles. However, the oscillating character of this interaction with a period of a few Å produces an overall minute effect over the entire volume of a nanoparticle and is therefore of secondary importance.

A series of experiments have revealed the importance of interparticle interactions and have brought about the necessity of a theoretical study of the magnetic properties of interacting magnetic nanoparticle assemblies. For example, in the limit of weak dipolar interactions, there has been a debate as to whether these interactions increase or decrease the blocking temperature of the system [9, 10], despite the fact that most experiments and simulations support the former behaviour. Furthermore, an open question remains as to whether blocking of the individual magnetic moments or a collective freezing due to interparticle interactions is the appropriate description of the low-temperature magnetic behavior. To this end a series of experiments and theoretical works have attempted to reveal similarities in the dynamical properties of fine particle assemblies (granular films, ferrofluids) and canonical spin glasses [8, 11]. The competing and frustrating character of the dipolar interactions in a random assembly (Fig.1) renders the analytical solution to the problem of determining the ground state intractable and inevitably leads to the implementation of numerical methods.

Granular films exhibit the phenomenon of Giant Magnetoresistance (GMR), namely a large decrease of the resistivity under application of a magnetic field. Above the blocking temperature and in the absence of an external magnetic field the magnetic moments point in random directions and the system has the maximum resistivity. Application of a magnetic field aligns the magnetic moments and the resistivity of the sample drops typically by ~10% relative to the zero field value. The GMR effect in granular metals is attributed to the same physical mechanisms as in the case of magnetic multilayers, namely the spin-dependent scattering of the conduction electrons off the magnetic particles [12, 13].

Experiments have revealed various factors that determine the size of the GMR effect. In particular, the value of GMR increases initially with increasing grain diameter and it decreases above a certain grain size. The maximum value occurs for particle diameters around the electron mean free path [13]. Varying the particle concentration, an optimum value is obtained around the percolation threshold [14]. Spin-dependent scattering in granular metals occurs predominantly at the magnetic/non-magnetic interface of the particle with the matrix and therefore the important role of the surface

structure of the particles has been underlined [15]. Finally, the optimum choice of the magnetic and the non-magnetic material for maximum GMR values remains an interesting issue [16]. Interparticle interactions can drastically modify the transport properties of nanoparticle assemblies through correlations in the magnetic moments of the grains. For completely decoupled grains the (magneto)resistance has a quadratic dependence on the sample magnetization [13] indicating that only the long-range magnetic order determines the size of the effect. However, many experimental groups have observed deviations from the parabolic dependence that have been attributed to interparticle interactions [17], to particle size distribution [13, 15] and to the coexistence of blocked and superparamagnetic particles [18] or collectively rotating and superparamagnetic particles [19] in the sample. The relative importance of these factors in producing the deviations from the inverted parabola are discussed in this article.

Finally, dipolar interactions between the magnetic particles are also of great importance during the growth process of the films. When magnetic particles diffuse on a substrate they move and relax their magnetic moments in a way that minimizes their mutual magnetostatic energy. The diffusion process is not a Brownian motion, but it is instead driven by the energetics of the interparticle interactions. When they unite, the morphology of the resulting aggregates is sensitive to the substrate temperature, the particle density and the strength of the interparticle interactions. At low particle concentrations (2-5%), it has been shown that magnetostatic forces between the particles lead to formation of aggregates with a complex morphology. The behavior of the magnetization and the magnetoresistivity under different external conditions (field, temperature) is a consequence of the morphology and size of the aggregates. A challenging task therefore emerges, namely to quantify the relation between the spatial correlations of the aggregates and their magnetic correlations, both long and short range.

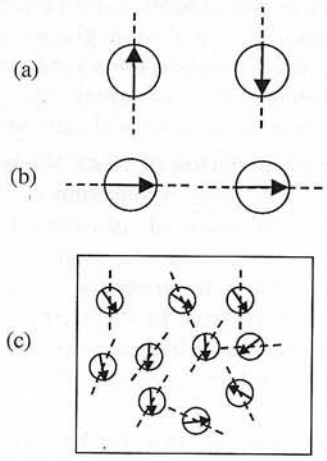

Figure 1. Ground state configuration of nanoparticles with magnetostatic (dipolar) interparticle interactions. Dashed line segments indicate the easy axes. (a) AF ordering of a pair of nanoparticles with easy axes perpendicular to the interparticle bond. (b) FM ordering of a pair of nanoparticles with easy axes along the interparticle bond (c) Frustrated ground state for a random assembly of nanoparticles with competing dipolar interactions.

The remainder of this article is organized as follows. In Section 2 we present the theoretical method we use to simulate the magnetic properties and the GMR effect in granular films. In Section 3 we discuss the hysteresis behavior and temperature dependent magnetization of granular films and nanoparticle aggregates. In Section 4 our results for the GMR effect in granular films and nanoparticle aggregates are presented and interpretation or relevant experimental findings is made. Some final remarks are made in Section 5.

2. Theoretical model and simulation method

2.1 Magnetic properties

The field and temperature dependence of the magnetic properties of random nanoparticle assemblies (granular films, FF, cluster assembled films) has been calculated [20, 21, 22] using the following model. The nanoparticles are spherical with diameter D and are located randomly inside a cubic box with edge length equal to LD and a typical value L=10. The particle assembly is assumed monodisperse in accordance with experimental evidence that both films formed by annealing [23] or grown by a cluster beam [21] are characterized by extremely low size dispersion (σ~5%). To avoid the overlap problem, the space inside the box is discretised by a simple cubic (or face centered) lattice with lattice constant equal to the particle diameter. The magnetic state of the each particle is described, according to the Stoner-Wolfarth model, by a classical spin vector ($\hat{S}_i$) with an anisotropy axis in a random direction ($\hat{e}_i$).The particles interact via long range dipolar forces and via exchange forces, when they are sufficiently close. The total energy of the assembly

$$E = g\sum_{i,j}\frac{\left(\hat{S}_i\cdot\hat{S}_j\right)-3\left(\hat{S}_i\cdot\hat{R}_{ij}\right)\left(\hat{S}_j\cdot\hat{R}_{ij}\right)}{R_{ij}^3} - J\sum_{\langle i,j\rangle}\left(\hat{S}_i\cdot\hat{S}_j\right) - k\sum_i\left(\hat{S}_i\cdot\hat{e}_i\right)^2 - h\sum_i\left(\hat{S}_i\cdot\hat{H}\right) \qquad (1)$$

where R_{ij} is the centre-to-centre distance between particles i and j, measured in units of the particle diameter. The energy parameters entering Eqn.(1) are the Zeeman energy $h=\mu H$, where $\mu=M_sV_o$ is the particle magnetic moment, the dipolar energy $g = \mu_0\mu^2/4\pi D^3$, the anisotropy energy $k=K_1V_o$ and the exchange energy J. The exchange coupling exists only between particles in contact (nearest neighbours). To model an infinite system, periodic boundaries are used and the dipolar interactions are summed using Ewald's method. The interplay between the four energy parameters (k,J,g,h) and temperature ($t=k_BT$) determines the equilibrium spin configuration of the assembly, which is obtained by a Metropolis Monte Carlo algorithm [24]. At a given temperature and applied field, the system is allowed to relax from an initial configuration towards equilibrium. The first 10^3 Monte Carlo steps per spin are used for thermalization of the system and the subsequent 10^4 steps are used to calculate thermodynamic averages. The results are averaged over 10-30 samples with different particle locations.

To calculate the remanence and the coercivity of a sample, the simulation starts with all spins pointing along the field axis and a saturating field H_s is applied. The field is gradually reduced with a constant step ΔH. The magnetization at H=0 is the required remanence (M_r) and the field value at which the magnetization is zero is the required

coercivity (H_c). The thermal history of a sample is obtained by drawing the zero-field-cooled (ZFC) and the field-cooled (FC) magnetization curves. This is completed in the following three stages : (i) the sample is initially at a high temperature (T_H) in the superparamagnetic regime (M=0) and is cooled at a constant rate (r_T) down to a very low temperature (T_L~0). This is a simulated annealing process that brings the system to the ground state. (b) A weak magnetic field is applied and the system is warmed up with the same temperature rate (r_T) to the highest temperature (T_H) and the ZFC curve is obtained. (iii) Without removing the field, the system is cooled down to T_L with the same rate (r_T) and the FC curve is obtained. For a dilute and monodisperse nanoparticle assembly, the ZFC/FC curves have a characteristic λ-shape with the bifurcation temperature corresponding to the blocking temperature of the nanoparticles. The deviations of the ZFC/FC curves from the λ-shape provide information about the energy barrier distribution in the sample [8]

For nanoparticle aggregates, we have developed a Diffusion Limited Cluster Aggregation algorithm to simulate the formation of dipolar interacting nanoparticle aggregates on an inert planar surface [25] and the resulting aggregate morphologies have been characterized by a fractal dimensionality. Next, the magnetic properties of these aggreagtes have been calculated [26, 27] using the Metropolis Monte Carlo algorithm described above.

2.2 Magnetotransport

When the electronic mean free path is longer than the particle diameter (λ>>D) a classical approach to the problem of spin-dependent transport and the related GMR effect in films containing magnetic nanoparticles, is adequate. Each magnetic particle introduces a local scattering potential which is proportional to the relative orientation between the local moment ($\hat{S}_i$) and the electron spin quantization axis [28]. The resistivity of the sample is then proportional to the short-range moment correlation function of sites within a distance not greater than the electron mean free path (λ) [27]

$$R(H)=R_0-R_1 f(H) \tag{2}$$

where R_0 and R_1 are material dependent parameters and

$$f(H)=\left\langle \hat{S}_i \cdot \hat{S}_j \right\rangle_\lambda \tag{3}$$

is the moment correlation function. For dilute granular metals at room temperature, λ is approximately equal to the centre-to-centre distance between adjacent particles [17] and therefore, the correlation function f(H) only for nearest neighbour particles is considered in Eqn.(3) . The magnetoresistance at field H is defined as

$$MR(H)=\frac{R(H)-R(H_S)}{R(H_S)} \tag{4}$$

where H is the applied field and H_s is the saturation field. The material dependent parameters R_0, R_1 enter the definition of MR and, in principle, they can be obtained by

fitting Eqn.(2) to the experimental results for a particular system. For non-interacting particles, the magnetic moments are uncorrelated, therefore $f(H)=(M/M_s)^2$, where $M/M_S = \langle \hat{S}_i \rangle$ is the normalized magnetization. Consequently, Eqn.(4) provides the observed parabolic dependence of MR on the sample magnetization. If the high field parabolic asymptote of the MR versus magnetization is subtracted from the MR values, one obtains the reduced magnetoresistance [17]

$$MR_r(H)=1-f(H) \tag{5}$$

which is obviously independent of the material parameters R_0, R_1 and serves as a universal curve whose deviations from a parabola indicate deviations from the superparamagnetic behaviour. Eqn.(5) indicates that the dependence of the MR on the micromagnetic configuration of the particle assembly enters via the short range moment correlation function. Monte Carlo simulations of the magnetic structure can therefore be directed implemented to obtain the reduced magnetoresistance [27].

Two important aspects not included in the previous formalism are the particle size dependence of the MR and the variation of the electronic mean free path with particle concentration. These two aspect are necessary in order to have a adequate description of the MR values over the whole range of magnetic volume fraction, namely from a dilute nanoparticle assembly to a continuous magnetic film. For this purpose we adopt a quantum description of the electronic magnetotransport [29]. We consider a finite sample of a granular solid with two semi-infinite electrodes attached to the opposite sides (Fig.2). The space occupied by the system is discretised by a cubic lattice with a constant equal to the nanoparticle diameter. The nanoparticles occupy the nodes of the lattice with probability p. We approximate the electronic structure of the granular system by a single-band Tight Binding Hamiltonian:

$$H = \sum_{i,\alpha} \varepsilon_i c_{i\alpha}^{+} c_{i\alpha} + V \sum_{<i,j>,\alpha} c_{i\alpha}^{+} c_{j\alpha} - J_0 \sum_{\substack{i \in MG \\ \alpha,\beta}} c_{i\alpha}^{+} \left(\hat{S}_i \cdot \hat{\sigma}\right)_{\alpha\beta} c_{i\beta} \tag{6}$$

Here i,j are the site labels, α,β are Cartesian coordinates, $c_{i\alpha}^{+}$ $(c_{i\alpha})$ is the creation (annihilation) operator of an electron with spin σ_α at site i, ϵ_i is the atomic potential on site i and it takes the values ϵ_{LW} in the electrodes, ϵ_{NM} in the non-magnetic matrix and ϵ_{MG} on the magnetic sites, V is the hopping integral between nearest neighbors <i,j> and is assumed uniform through the system, J_0 is the exchange potential on the magnetic sites and σ_α are the Pauli matrices. The third term in Eqn.(6) is the spin-dependent scattering potential that leads to the GMR effect. Its strength depends on the angle between the electronic spin and the local magnetization axis and this gives it a dependence on the externally applied magnetic field.

We describe the total system composed of the left electrode, the sample and the right electrode as a sequence of L layers with an in-plane LxL supercell. Using the Green function, $G^{\pm}(E) = (E - H \pm i0)^{-1}$, for the Hamiltonian given by Eqn.(6) one can express

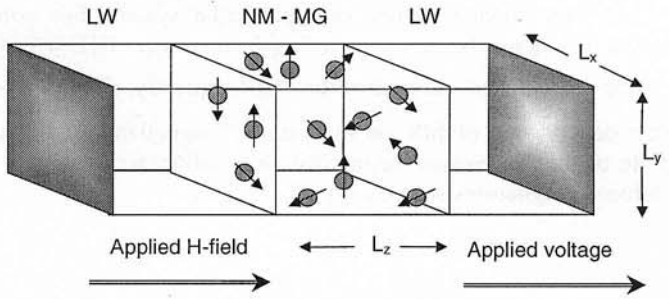

Figure 2. Sketch of the geometry used to calculate the conductivity of a granular film. LW=lead wire, NM-MG=heterogeneous mixture of magnetic particles (MG) in a non-magnetic (NM) matrix

the electronic conductivity of the system by the Kubo-Greenwood formula, which takes the form

$$\Gamma(E)=\frac{2e^2V^2}{h}\mathrm{Tr}\begin{pmatrix}\tilde{G}(k,k)\cdot\tilde{G}(k-1,k-1)+\tilde{G}(k-1,k-1)\cdot\tilde{G}(k,k)-\\ \tilde{G}(k,k-1)\cdot\tilde{G}(k-1,k)-\tilde{G}(k-1,k)\cdot\tilde{G}(k,k-1)\end{pmatrix} \tag{7}$$

where $\tilde{G}=\mathrm{Im}\,G^{+}$ and k is the layer index. The magnetic structure of the granular sample enters the expression for the conductivity through the spin-dependent term of the Hamiltonian in Eqn.(6). The calculation of the conductivity, via Eqn.(7), is implemented in the Monte Carlo relaxation procedure for the magnetic structure and eventually the thermal average of the conductivity over many equilibrium micromagnetic states is obtained [29].

3. Magnetic properties

3.1 Random nanoparticle assemblies

At first, we neglect the interparticle exchange coupling, by setting J=0 in Eqn.(1), and study the variation of the hysteresis characteristics (remanence and coercivity) with particle concentration [20]. At low temperature ($t/k \sim 10^{-3}$), these show a rather complex behaviour that is controlled by the relative strength of the intraparticle anisotropy (k) to the interparticle dipolar interactions (g). A purely dipolar assembly shows a maximum in the remanence and the coercivity (Fig.3) around the percolation threshold. This behaviour is the combined effect of two factors, namely, the sensitivity of the dipolar interactions on the spatial arrangements of the moments and the ramified structure of the system close to percolation. In the limit of ideal packing ($x_V=\pi/6$ for a SC lattice) the stacking geometry favors a columnar antiferromagnetic structure in the ground state and therefore both M_r and H_c vanish. In systems with weak dipolar coupling ($g/k<1$) an enhancement of the remanence is seen followed by a reduction of the coercivity. In this regime, dipolar interactions render the system magnetically softer. This behaviour is attributed to the macroscopic Lorentz field acting on each dipole. In contrast to this trend, when free boundaries exist, the remanence is suppressed with increasing particle density (Fig.3) due to the sample depolarizing field. Therefore, the role of boundaries is

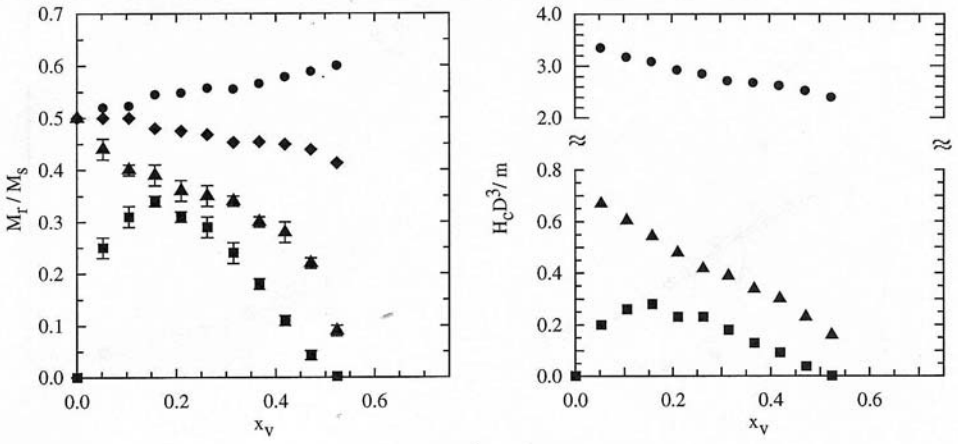

Figure 3. Dependence of remanence (left) and coercivity (right) on the metal volume fraction $x_V=(\pi/6)p$ (p=occupation probability) at low temperature ($t/k=10^{-3}$). Squares : dipolar particles (g=1, k=0). Triangles: moderate coupling (g=k=1). Circles: weak coupling (g=1, k=4). Diamonds: weak coupling (g=1, k=4) and free sample boundaries. Not indicated error bars are of the size of the marks.

crucial in dipolar interacting nanoparticle assemblies. Finally, in the moderate coupling regime (g/k~1) a reduction of both the remanence and the coercivity with particle concentration is found, with an almost linear dependence as Néel's mean-field arguments predict [30]. Magnetization measurements at low temperature on FF showed suppression of the remanence (M_r/M_s~0.2) for moderately interacting samples (g/k~1) [31] and enhancement of the remanence (M_r/M_s>0.5) for weakly interacting samples (g/k~0.34) [32]

The temperature dependence of the remanence and coercivity shows the transition from the thermally stable (blocked) to the superparamagnetic regime as both quantities vanish for temperatures above the blocking. Comparison of the temperature dependence of the remanence and the coercivity (Fig.4) with the corresponding curves for non interacting nanoparticles (g=0) reveals the complex role of the dipolar forces. With reference to the blocking temperature of the non-interacting assembly predicted by our simulations [33], it is shown (Fig.3) that at low-temperatures ($T < T_b^0$), dipolar interactions have a demagnetizing effect revealed by a suppression of the remanence and the coercivity. In contrast to this, at high temperatures ($T < T_b^0$) dipolar interactions stabilize a ferromagnetic behaviour, leading to finite values of the remanence and coercivity. In this temperature regime a dipolar ferromagnetism is induced in the random assembly of nanoparticles. In a single-particle picture, dipolar interactions suppress the average energy barrier for magnetization reversal at low temperature, but they enhance the same barrier at elevated temperature. The high temperature behaviour of dipolar interactions in random nanoparticle assemblies is in agreement with the results of mean-field theory [9], while the increase of the effective average barrier with temperature has been recently verified [34] by a numerical path integral method. A series of experiments in granular films [9] and in FF [31] are in agreement with the simulation predictions,

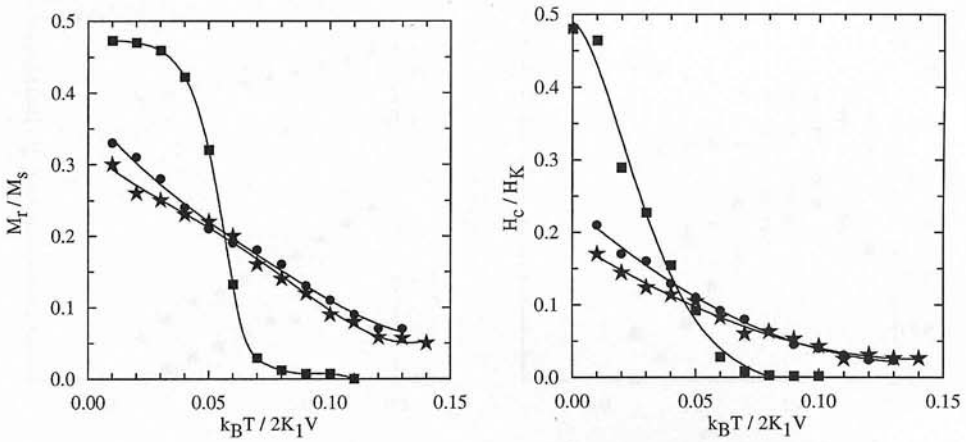

Figure 4. Temperature dependence of remanence (left) and coercivity (right). Squares : non-interacting particles (k=1,g=0) Stars : dipolar interacting nanoparticles (k=g=1) with x_v=0.157. Circles : dipolar interacting particles (k=g=1) with x_v=0.314. Solid lines are guides to the eye. Error bars are of the size of the marks.

indicating a clear increase of the blocking temperature with increasing particle concentration.

A second important factor that enhances the blocking temperature of a nanoparticle assembly is the distribution in the particle sizes [35, 36]. Using a percolation algorithm we have generated clusters of particles on a simple cubic lattice with concentration (x=0.25) close to the percolation threshold. In this concentration regime, the distribution of cluster sizes behaves as f(nc)~nc-a and clusters of all sizes exist in the sample. All particles belonging to the same cluster rotate coherently under an applied field, thus the cluster is treated as a Stoner-Wolfarth particle with random shape and a random easy axis attributed to it. The cluster size distribution implies a distribution in the energy barriers of the individual clusters and therefore at intermediate temperatures a mixture of superparamagnetic and blocked clusters exists. This new feature modifies drastically the temperature dependence of the magnetic properties with respect to the monodisperse samples mentioned above. Comparison of the temperature dependent remanence for this polydisperse sample and a corresponding monodisperse one with the same average cluster size (Fig.5) shows that both the size distribution of the clusters and the dipolar interactions between them introduce a distribution of energy barriers in the system and lead to a slow decay of the remanence with temperature and an enhancement of the blocking temperature. However, below the blocking temperature, the sample morphology is crucial. Reduction of the remanence due to interactions is seen in the monodisperse sample while enhancement of the remanence is observed in the polydisperse system. This behaviour originates from the presence of a few very large clusters in the polydisperse sample, that are blocked and produce a strong local magnetic field that causes an efficient alignment of the small clusters.

When nanoparticles are in contact, the overlap of the surface electronic states leads to an exchange interaction between them. Assuming that the surface of a nanoparticle is

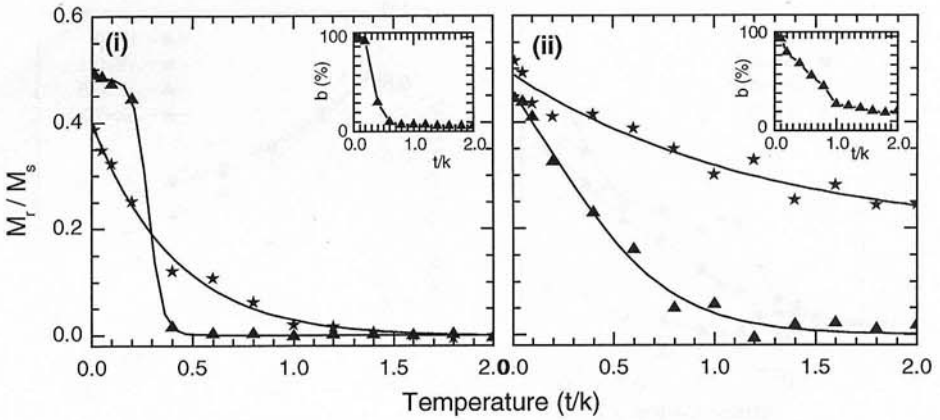

Figure 5. Temperature dependence of the remanence for (i) monodisperse and (ii) polydisperse samples containing coherent clusters. The monodisperse sample contains coherent clusters of size n_c=3 and the polydisperse one has an average cluster size $\langle n_c \rangle$=3.1±19%. Stars : non-interacting clusters (k=1,g=0). Triangles : dipolar interacting clusters (k=g=1). Insets: Fraction of blocked moments as a function of temperature for the non-interacting samples (g=0). Concentration of magnetic particles x=0.25. Solid lines are guides to the eye.

in a ferromagnetic state, it is anticipated that the nature of the interparticle exchange interaction will also be of the same nature. Evidence of ferromagnetic interparticle exchange interactions has been provided recently for granular systems close to percolation [37] and studied in the weak-J limit by Monte Carlo simulations [38]. However, films grown by a cluster beam technique provided evidence that strong interparticle exchange is present [21]. Motivated by these experiments we have studied the magnetic behaviour over the whole range of exchange constants values, thus modelling the transition from well separated (J=0) to coalesced (J/k>>1) particles [22].

The low temperature dependence of the remanence and coercivity on particle concentration reveals the competing character of the exchange and dipolar interactions (Fig.6). The former favour enhancement of the remanence while the latter suppress the long range order. A crossover in the trend of the remanence behaviour is observed when the strengths are comparable (J~g). In contrast to this behaviour, the coercivity is always suppressed by interparticle interactions. The suppression is more dramatic when the particles coalesce (J>>k), because in this case the emerging cluster is still in a single-domain state but with a reduced anisotropy arising from averaging upon the easy axes directions of the merging clusters.

Further simulations on Fe clusters embedded in Ag matrix by a low-energy cluster beam deposition technique [21] revealed that strong interparticle exchange exists for concentrations close to percolation. The evolution of the FC/ZFC magnetization curves with Fe concentration in the temperature range 2-350K is shown in (Fig.7). For the dilute sample (p~1%) a sharp peak of the ZFC curve occurs at the blocking temperature and a Curie behavior (M~1/T) is shown at temperatures well above the blocking ($T \gg T_b$). Finally, a weak variation of Tb with applied field (~15%) is found, which is in

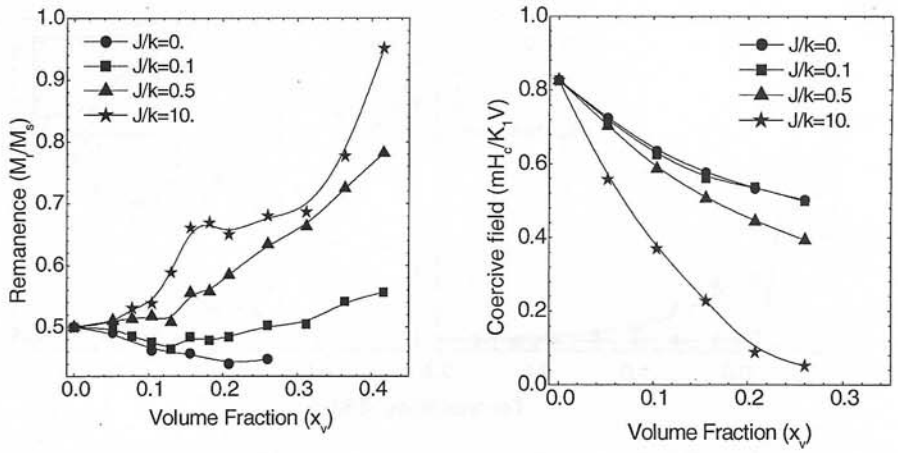

Figure 6. Dependence of remanence on metal volume fraction for an assembly of exchange and dipolar interacting nanoparticles at low temperature (t/k=0.01) for various interparticle exchange strengths (J/k) and dipolar strength g/k=0.65.

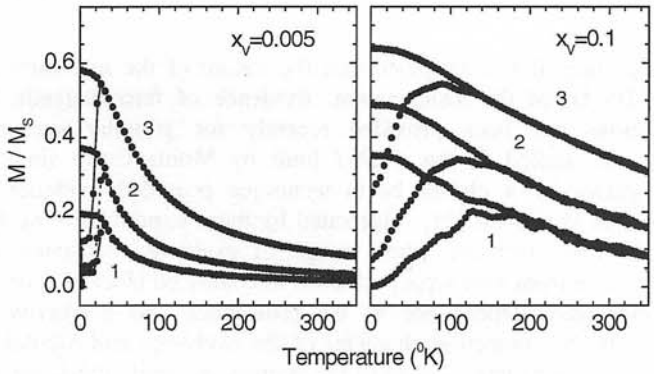

Figure 7. Zero-field-cooled and field-cooled curves of Fe cluster-assembled film in the dilute limit (left panel) and close to percolation (right panel). Labels 1,2,3 correspond to applied field values of 100 G, 200 G and 500 G, respectively. Parameters for Fe nanoparticles : diameter D=3nm, saturation magnetisation M_s=1.7x10^6 A/m, anisotropy density K_1=2.4x10^5 J/m^3 and (interparticle) exchange coupling J=3.1x10^{-20}J

agreement with a mean-field model [39] that predicts a 10-30% variation of T_b for H=100-500G. These features indicate that the dilute sample is a non-interacting assembly. The magnetization curves are drastically different in the dense sample (Fig.7). The maximum of the ZFC curve is broad indicating a wide distribution of energy barriers in the system. At high temperature ($T \gg T_b$) the dependence is almost linear, deviating seriously from the Curie law. Finally, the position of the ZFC peak is very

sensitive to the applied field, as designated by the large up-shift (~50%). These features of the FC/ZFC curves are in good agreement with experimental measurements in Fe cluster assembled films [21]. The physical picture drawn from these results is that exchange interactions couple individual clusters into (coherent) aggregates giving rise to the increase in T_b and the aggregates interact via dipolar forces that produce the strong field dependence of Tb and the almost linear decay of the magnetization with temperature.

3.2 Nanoparticle aggregates

In ferrofluids the particles are mobile at temperatures above the freezing point of the solvent and they tend to form agglomerates with complex morphology [40]. Similar structures are formed when magnetic colloidal microspheres are allowed to diffuse on a planar surface [41]. The formation of these complex aggregate morphologies is driven by the magnetostatic interparticle interactions. The formation of these aggregates implies the existence of spatial correlations in the nanoparticle assembly. We have investigated the impact of these correlations in the magnetic properties of the aggregates. To this end we modelled the aggregation of spherical magnetic nanoparticles on a planar substrate by a diffusion limited cluster aggregation process (DLCA) on a triangular lattice [25]. The final aggregate morphology has been characterised by a fractal dimensionality and our simulations yielded D_f=1.23±0.04 for aggregates formed at low temperature (relative to the dipolar interaction energy) and low coverage density (~2%). This value of D_f shows the tendency of the particles to form chain-like aggregates and the ground state magnetic structure is a nose-to-tail arrangement of the magnetic moments.

The field-dependent magnetisation of these aggregates shows a finite-size scaling behaviour (Fig.8) described by the relation

$$M_N(H) = a(H) + b(H)N^{-1/D_f} \tag{8}$$

where N is the number of particles composing the aggregate and D_f the fractal dimensionality [26]. This relation is a generalization of the corresponding expression for the finite-size effects for a Euclidean object (N=integer), where a thermodynamic quantity is made out of a bulk (N- independent) and a surface (N-dependent) contribution. Since D_f is determined solely by the growth conditions (particle density, temperature), the importance of Eqn.(8) lies in the fact that its integral over the aggregate size distribution provides directly the magnetisation of an aggregated sample.

Fractal objects, in general, belong to a wider class of self-organized critical systems, that is, systems in which the criticality arises without tuning of a driving force. Hence, applying a weak field to these systems is equivalent to applying this field to a (Euclidean) magnetic system at the critical point. One therefore expects that the magnetization of (fractal) aggregates will follow a scaling law of the form $M \sim H^{1/\delta}$, with the critical exponent $\delta>1$ [42]. Indeed our numerical simulations [43] verified this behaviour and predicted an exponent δ=4.4+0.4 (Fig.8), which lies well above the predictions of mean field theory (δ=3). An important consequence of this scaling law is that the low-field susceptibility of a system containing nanoparticle aggregates will diverge at zero-field ($\chi \sim H^{0.77}$) expressing the collective response of the aggregate.

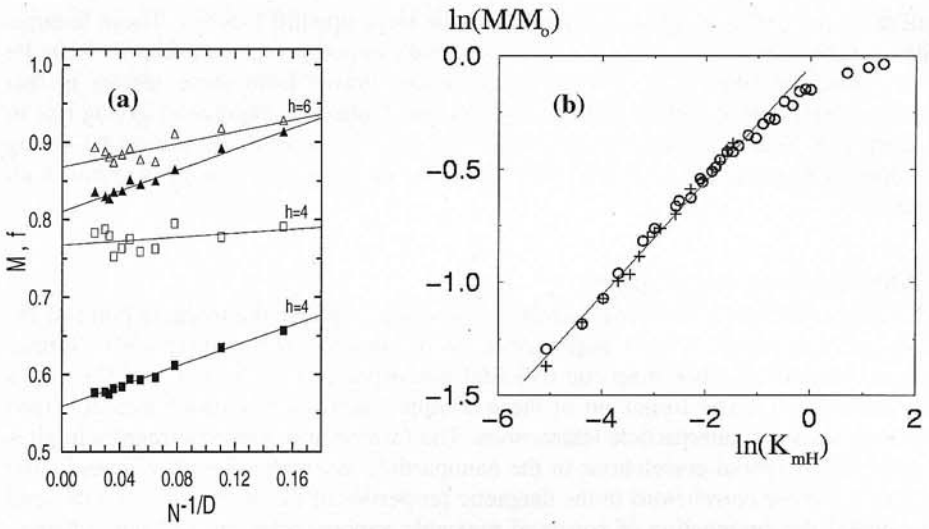

Figure 8. (a) Dependence of magnetization (full symbols) and short-range correlation function (open symbols) on the linear size of the aggregate. Applied field (h) is normal to the substrate. Squares : h=4 and triangles: h=6. Solid lines are a linear fit to the data. (b) Power-law dependence of the magnetization on applied field (K_{mH}=h/g) for two-dimensional aggregates with size N=32 (crosses) and N=64(circles). The straight line is a linear fit corresponding to a critical exponent $1/\delta=0.23\pm0.02$

4. Magnetotransport

4.1 GMR in random assemblies of nanoparticles

The spin-dependent conductivity of a granular metal was calculated [29, 35, 36] within the quantum formalism of Eqn.(7). The following choice was made for the electronic structure parameters entering the electron Hamiltonian, Eqn.(6). The hopping integral is constant throughout the electrodes and the granular sample and it defines the energy scale (V=1.0). Consequently, the bandwidth in all materials (electrode, matrix, magnetic grain) is W=12 and equivalently, the electron effective mass in the electrodes, the non-magnetic matrix and the magnetic grains is constant. The on-site potentials in the electrodes and in the non-magnetic matrix are equal, $\epsilon_{LW}=\epsilon_{NM}=0$, to remove the possibility of contact resistance. On the magnetic sites we choose $\epsilon_{MG}=+2$ and $J_0=+2.0$, so that the electrons in the majority spin band are less scattered at the magnetic grains than those in the minority band, when the magnetic moments of the grains are aligned ferromagnetically. This choice of parameters introduces in our model the essential aspect of asymmetry in spin-dependent scattering that has been observed in Co/Cu magnetic multilayers and that is expected to be valid for granular CoCu alloys [44]. The Fermi level is set at the band centre ($E_F=0$) giving the conduction electrons a wavelength comparable to the grain size ($\lambda_F\approx D$). The energy parameters that determine the micromagnetic configuration correspond to Co nanoparticles with diameter D=3.5nm, saturation magnetisation M_s=1500 emu/cm^3, and anisotropy density $K_1=1.2\times10^6$ erg/cm^3. The exchange coupling between nanoparticles is neglected at this stage. These values

correspond to g/k~1 and J=0 for the parameters of Eqn.(1). Polydisperse samples are generated by a percolation algorithm as discussed earlier (Section 3).

The field dependent magnetoresistance of an initially demagnetised sample (anhysteretic curve) (Fig.9) shows the characteristic maximum at zero field and it tends to zero when all moments tend to align parallel to the applied field. The maximum MR value is suppressed due to interparticle interactions. These introduce ferromagnetic correlations between the magnetic moments and they reduce the random order, which is the prerequisite for maximum resistance at zero field. Furthermore, the saturation of MR occurs at higher fields when interactions are switched on, reflecting the weaker response of the interacting system to the external field. For an effective alignment of a magnetic moment, the Zeeman energy due to the external field must overcome the thermal noise. If, however, the moments are dipolar coupled, it must also overcome the anisotropic dipolar interaction energy with all the other moments of the system. This effect explains the higher saturation field observed (Fig.9). The final outcome is a reduction of the sensitivity of the MR effect to the external field when the particles are dipolar coupled. A small rounding of the MR-H curve around the zero field in the case of strong dipolar interactions (marked by circles in Fig.9) is an additional demonstration of the domination of the interparticle interactions over a weak external field in rotating the magnetic moments.

To clarify the relative importance of the interaction effects and the particle size distribution in the suppression of the GMR effect consider the following argument. At the temperature of the simulation (t/k=1.2) the polydisperse sample contains a mixture of blocked and superparamagnetic clusters (b~0.25 in Fig.5), while the monodisperse sample contains only superparamagnetic clusters (b~0 in Fig.5). Both systems have similar values of MR (~19%), when the dipolar interactions are neglected, which indicates that the large and blocked clusters of the polydisperse sample do not contribute to the GMR effect, a fact that was expected from the imposed condition that the electron

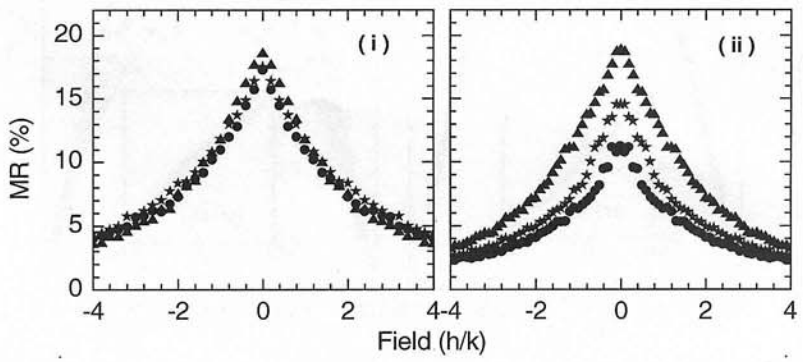

Figure 9. Anhysteretic field dependence of the magnetoresistance for a granular metal. (i) monodisperse sample containing coherent cluster of size n_c=3 and (ii) polydisperse sample containing coherent cluster of average size $\langle n_c \rangle$=3.1±19% and, both with x_v=0.25 at t/k=1.2 (see Fig.5X). Triangles: non-interacting anisotropic particles (k=1,g=0). Stars : dipolar interacting anisotropic particles (k=g=1). Circles : dipolar interacting isotropic particles (k=0,g=1).

Fermi wavelength is much smaller than these clusters (λ_F~1 and D_{max}~20). When the interactions are switched on, a larger suppression of the GMR effect is observed in the polydisperse sample (MR~14%) compared to the monodisperse (MR~18%). This happens because the large clusters that exist in the polydisperse sample produce strong magnetostatic fields that lead to an efficient ferromagnetic alignment of the smaller clusters surrounding them. These correlations are responsible for the suppression of the GMR effect and they are enhanced by the presence of a few large moments in the sample. The role of the dipolar interactions when large clusters are present is clarified further by the results for the polydisperse sample when the uniaxial anisotropy is neglected (circles in Fig.10). Then a more severe flattening of the MR curve is seen, because the ferromagnetic correlations between the moments are not destructed by the uniaxial anisotropy of the individual cluster. Similarly large flattening of the MR-M curves with increasing particle polydispersity has been observed in measurements of MR in CoCu films [17]. Large flattening of the MR curve has also been observed in discontinuous CoCu multilayers containing fragmented Co layers [45]. In these samples, ferromagnetic correlations exist at zero field, which are in analogy to the to the dipolar interactions-induced correlations in random nanoparticle assemblies (granular films).

Finally, using the percolation model and defining coherent clusters as discussed previously (Section 3) we study the dependence of the magnetoresistance on the magnetic content of the sample. The zero-field MR shows a characteristic peak around

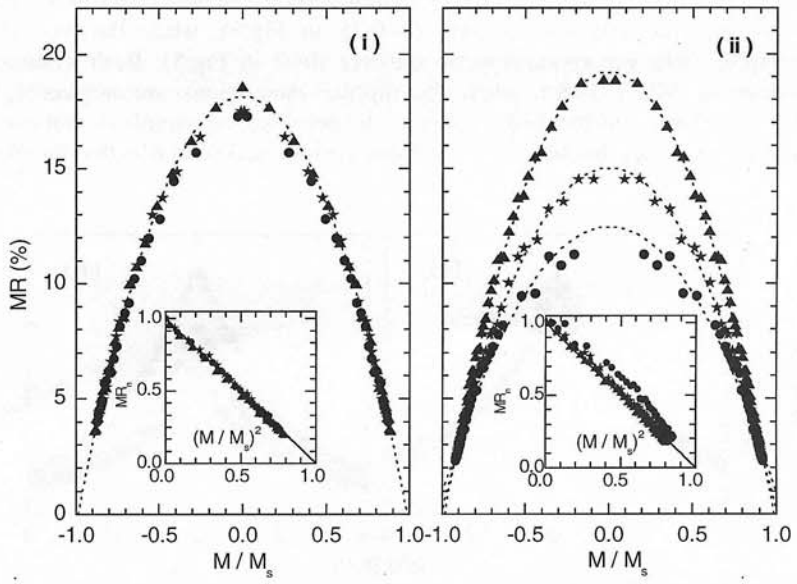

Figure 10. Dependence of magnetoresistance on magnetisation. For a (i) monodisperse and (ii) polydisperse sample, both with x_v=0.25 at t/k=1.2 (see Fig.5X). Triangles: non-interacting anisotropic particles (k=1,g=0). Stars : dipolar interacting anisotropic particles (k=g=1). Circles : dipolar interacting isotropic particles (k=0,g=1). Dashed lines show the parabola fitted to the high-field data. Insets show the same MR data drawn versus the square of magnetisation. The straight line in the inset is the theoretical prediction for non-interacting monodisperse samples.

the percolation threshold (x_p) (Fig.11). The existence of an optimum concentration for the GMR effect is the result of the competition between two competing factors. Namely, the increasing number of magnetic scattering centres that enhance the GMR effect and the increase of the average cluster size that suppresses the effect. Alternatively, since spin-dependent scattering occurs only at the magnetic-non magnetic interface, the evolution of MR with concentration reflects the evolution of the total magnetic-non magnetic interfacial area (A) in the sample. Indeed the calculated A-x_v curve [46] fitted very well the MR-x_v in the concentration regime below the percolation threshold. Dipolar interactions have two effects on the concentration dependence of MR. First, they suppress the MR values, especially close to x_p (Fig.11), leading to a faster decay with magnetic particle concentration. Second, the peak of MR appears at slightly lower concentration. Both these effects are attributed to the ferromagnetic correlations introduced by dipolar interactions, which destroy the random order of the moments at zero field. Close to percolation, the ramified morphology of the sample induces longer range correlations and therefore a stronger suppression of the MR values. The shift of the MR peak occurs because strong dipolar interactions extend the region of magnetic coherence well beyond the natural borders of each magnetic cluster, therefore the scattering region is larger than the cluster size.

As regards the experimental findings, granular samples grown by various techniques (cluster beam deposition [14,46], sputtering [47, 48]) exhibit the same characteristic maximisation of the MR value around the percolation threshold. A shift of the MR peak to lower concentrations with decreasing temperature has been measured [48] and attributed to the increasing role of interparticle dipolar interactions.

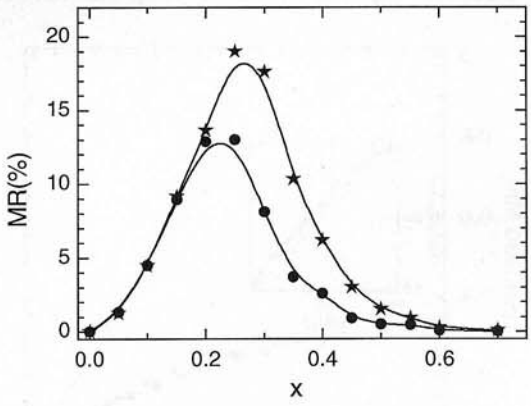

Figure 11. Dependence of zero-field magnetoresistance on magnetic content in the granular sample. Stars : non-interacting clusters (k=1,g=0). Circles: dipolar interacting clusters (k=g=1). Solid lines are guides to the eye. The maximum of MR occurs close to the percolation threshold (x_p~0.3)

4.2 GMR in nanoparticle aggregates

Giant magnetoresistance in magnetic nanoparticle assemblies is sensitive to the magnetic correlations existing in the sample. These are determined by the strength and the nature of the interparticle interactions. Dipolar interactions are sensitive to the spatial arrangement of the nanoparticles. It is therefore an interesting issue to examine the

behaviour of the GMR effect in nanoparticle aggregates that are characterised by long-range spatial correlations (see Section 3).

We have calculated [27] the reduced magnetoresistance Eqn.(5), for a granular sample containing well separated two-dimensional aggregates. Within each aggregate the particles are in contact and they interact strongly with each other, mainly through dipolar forces. The effective exchange interaction is neglected at this stage. In a dilute sample, dipolar interactions between particles belonging to different aggregates are weak due to the spatial separation of the aggregates and have also been neglected. Therefore, it is realistic to approximate the granular film by a collection of uncoupled aggregates with dipolar interactions between their constituent particles. Finite-size effects are expected to be important for the field-dependent short-range correlation function of an aggregate, Eqn.(3), in complete analogy to scaling behaviour of the magnetization (Section 3). Using a large number of aggregates (N~6000) we have shown that the correlation function obeys the scaling relation

$$f_N(H) = a_f(H) + b_f(H) N^{-1/D_f} \tag{9}$$

where N is the size of the aggregate (Fig.8). Thus, the fractal dimensionality that characterizes the spatial morphology of the aggregates is a suitable exponent to describe the finite size effects of the giant magnetoresistance. We have also found that strong ferromagnetic correlations exist in a system containing chain-like aggregates of magnetic particles leading to serious suppression of the MR_r (~30%) values at zero-field and deviations from the parabolic dependence on the magnetisation (Fig.12). In granular

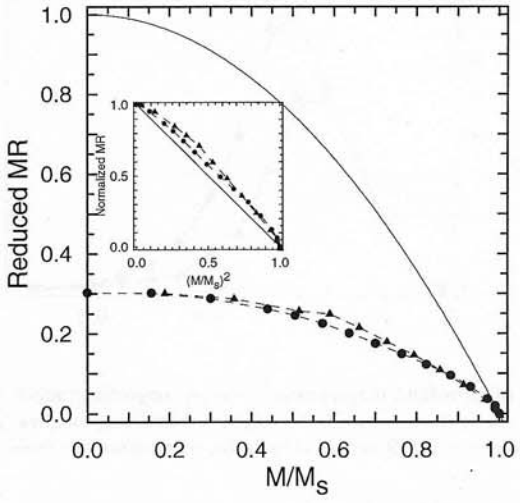

Figure 12. Dependence of magnetoresistance on magnetisation showing a large suppression at low fields. The samples contain magnetic aggregates of uniform size coupled by strong dipolar interactions (g/t~100). Finite-size effects are demonstrated by comparison of the data for small (N=10, triangles) and large (N=100, circles) aggregates. The non-interacting limit (g=0) is shown by the $1-(M/M_s)^2$ parabola (solid line). Inset : Deviations from the parabolic MR vs. M dependence.

films close to percolation, particle coalescence can lead to formation of elongated particles that have a magnetic behaviour similar to chain-like aggregates. In recent experiment [49] the observed reduction of the MR values has been attributed to formation of chain-like clusters. This remark underlines the relevance of our study of magnetic aggregates to granular systems close to percolation.

5. Final remarks

The magnetic and magnetotransport properties of nanoparticle assemblies (granular films, cluster assembled films, ferrofluids) are governed by the delicate interplay between the single-particle magnetic characteristics and the interparticle interaction effects. Although the former find a satisfactory almost analytical description within the coherent rotation model of Stoner-Wolfarth, the analytical approach for interacting systems has a limiting validity especially in high density samples, which attract most of the current research interest. In our work, we have addressed the effects of interparticle interactions on the magnetic and magnetotransport properties of magnetic nanoparticles combining Monte Carlo simulations and electronic transport theory.

There are still open questions in the field of magnetic nanoparticle assemblies. The nature of the ground state of a dipolar interacting random assembly of nanoparticles [8], the slow thermal decay of the magnetization in nanoparticle assemblies and the corresponding relaxation mechanism [50], the response of nanoparticles to time-dependent applied fields and the corresponding dynamic coercivity [1], the mechanism of charge transport in magnetic granular insulators and the related tunnelling magnetoresistance effect [51] are a few of the problems related to the physics and technological exploitation of magnetic nanoparticle assemblies. Numerical methods of statistical physics (Monte Carlo, Langevin dynamics, Fluctations theory) combined with condensed matter methods (transport theory, electronic structure) provide an efficient theoretical tool to investigate these phenomena.

Acknowledgments

We would like to acknowledge useful discussions with Prof. J. A. Blackman, Prof. Sir R. J. Elliott, Prof. C. Binns and Prof. P. Allia. This work was supported by a GROWTH Project (No. G5RD-CT-2001-00478) and a Bilateral Greece-Great Britain program (No. 10807/202).

References

1. D. Weller and A. Moser, IEEE Trans. Magn., **35**, 4423 (1999)
2. K. J. Kirk, Contemp. Phys., **41**, 61 (2000)
3. E. Blums and R.E. Rosensweig J. Magn. Magn. Mat., **85** 303 (1990)
4. E. C. Stoner and P. Wolfarth, Philos. Trans. R. Soc. London, Ser. A **240**, 599 (1948)
5. L. Néel, Compt. Rend., **228**, 664 (1949); Ann. Geophys., 5, 99 (1949)
6. C. P .Bean and J. D. Livingston, J. Appl. Phys., **30**, 120 (1959)
7. J.L.Dormann and D.Fiorani (eds.), *Magnetic Properties of Fine Particles* (North-Holland, Amsterdam, 1992)
8. J.L.Dormann, D.Fiorani and E.Tronc, Adv. Chem. Phys., **98**, 283 (1997)
9. J. L. Dormann, L. Bessais and D. Fiorani, J. Phys. C: Cond. Matter, **21**, 2015 (1988)
10. S.Mørup and E.Tronc, Phys. Rev. Lett., **72**, 3278 (1994)

11. X. Batlle and A. Labarta, J. Phys. D : Appl. Phys., **35**, R15 (2002)
12. A. E. Berkowitz, J. R. Mitchell, M. J. Carey, A. P. Young, S. Zhang, F. E. Spada, F. T. Parker, A. Hutten, and G. Thomas, Phys. Rev. Lett. **68**, 3745 (1992)
13. J. Q. Xiao, J. S. Jiang and C. L. Chien, Phys. Rev. Lett. 68, 3749 (1992)
14. F. Parent, J. Tuaillon, L. B. Stern, V. Dupuis, B. Prevel, A. Perez, P. Melinon, G. Guiraud, R. Morel, A. Barthelemy, and A. Fert, Phys. Rev. B **55**, 3683 (1997).
15. E. F. Ferrari, F. C. S. da Silva and M. Knobel, Phys. Rev. B **56**, 6086 (1997).
16. A. Fert and P. Bruno, in *Ultrathin Magnetic Structure II*, edited by B. Heinrich and J. A. C. Bland (Springer Verlag, Berlin, 1994), p. 82.
17. P. Allia, M. Knobel, P. Tiberto, and F. Vinai, Phys. Rev. B **52**, 15398 (1995).
18. B. J. Hickey, M. A. Howson, S. O. Musa, and N. Wiser, Phys. Rev. B 51, 667 (1995).
19. J. F. Gregg, S. M. Thompson, S. J. Dawson, K. Ounadjela, C. R. Staddon, J. Hamman, C. Fermon, G. Saux and K. O' Grady, Phys. Rev. B **49**, 1064 (1994)
20. D. Kechrakos and K. N. Trohidou, Phys.Rev. B **58**, 12169 (1998)
21. C. Binns, M. J. Maher, Q. Pankhurst, D. Kechrakos and K. N. Trohidou, Phys. Rev. B **66**, 184413 (2002)
22. D. Kechrakos and K. N. Trohidou, J. Magn. Magn. Mater. **262**, 107 (2003)
23. C.L.Chien, in *Science and Technology of Nanostructured Magnetic Materials*, edited by G.C. Hadjipanayis and G.A. Prinz (Plenum Press New York, 1991) NATO ASI Series, Series B, Vol. **259**, p.477
24. K.Binder and D.W.Heermann, *Monte Carlo Simulation in Statistical Physics* (Springer Verlag, Berlin, 1988) Springer Series in Solid-State Sciences, Vol. 80.
25. K. N. Trohidou and J. A. Blackman, Phys. Rev. B **51**, 11521 (1995)
26. K. N. Trohidou and D. Kechrakos, J.Phys.:Cond.Matter, **10** L255 (1998)
27. D. Kechrakos, K.N. Trohidou and J. A. Blackman, Phys. Rev. B **63**, 134422 (2001)
28. P. M. Levy, Solid State Physics (H. Ehrenreich and D. Turnbull, Eds., Academic Press, Inc., New York), **47**, 367 (1994).
29. D. Kechrakos and K. N. Trohidou, Phys.Rev. B **62** 3941-3951 (2000)
30. See, for example, B. D. Cullity, *Introduction to Magnetic Materials* (Addison-Wesley, Reading, MA, 1972)
31. W Luo, S R Nagel, T F Rosenbaum and R E Rosensweig, Phys. Rev. Lett., 67, 2721 (1991)
32. S. Mørup, F.Bodker, P.V.Hendriksen, and S.Linderoth, Phys. Rev., B **52**, 287 (1995)
33. Our simulation predict $T_b^o \sim 0.16(K_1V/k_B)$ for non-interacting nanoparticles, while most experiments give $T_b^o \sim 0.04(K_1V/k_B)$. Being a non-equilibrium quantity, the blocking temperature depends on the time scale used for measuring or simulations it. For a relevant discussion on the estimation of T_b using MC simulations, see for example, D. A. Dimitrov and G. M. Wysin, Phys. Rev. B **54**, 9237 (1996)
34. D. V. Berkov, J. Magn. Magn. Mater., **186**, 199 (1998); *ibid*, IEEE Trans. Magn., **38**, 2637 (2002)
35. D. Kechrakos and K.N. Trohidou, Phys. Stat. Sol. (a) **189**, 277 (2002)
36. D. Kechrakos and K.N. Trohidou, Physica B **318**, 360 (2002)
37. V. Franco, X. Batlle, A. Labarta and K. O' Grady, J. Phys. D : Appl. Phys., 33, 609 (2000)
38. C. Verdes, B. Ruiz-Diaz, S. M. Thompson, R. W. Chantrell and Al. Stancu, Phys. Rev. B, 65, 174417 (2002)
39. J.L.Dormann, D.Fiorani and M.El Yamani, Phys. Lett., A **120** , 95 (1987)
40. S.Menear, A.Bradbury and R.W.Chantrell, J. Magn. Magn. Mater., 43, 166 (1984)
41. S. Helgesen, A. T. Skjeltrop, P. M. Mors, R. Botet a,d R. Jullien, Phys. Rev. Lett., **61**, 1736 (1988)
42. H. E. Stanley, *Introduction to phase transitions and critical phenomena*, (Oxford University Press, 1971)

43. R. Botet, K. N. Trohidou, J. A. Blackman and D.Kechrakos, Phys. Rev. E **64**, 031401 (2001)
44. Y. Asano, A. Oguri, J. Inoue, and S. Maekawa, J. Magn. Magn. Mater. **140-144**, 505 (1995)
45. P. Vavassori, E. Angeli, D. Bisero, F. Spizzo and F. Ronconi, J. Magn. Magn. Mater. **262**, 52 (2003)
46. S. Rubin, M. Holdenried and H. Micklitz, Eur. Phys.J., B **5**, 23 (1998)
47. M.M. Pereira de Alzevedo, G. N. Kakazei, A. F. Kravetz, V. S. Amaral, Yu. G. Pogorelov, and J. B. Sousa, J. Magn. Magn. Mater. 196-197, 40 (1999).
48. F. Spizzo, E. Angeli, D. Bisero, F. Ronconi, P. Vavassori, P. Allia, V. Selvaggini, M. Coisson, P. Tiberto and F. Vinai, J. Magn. Magn. Mater. **262**, 88 (2003)
49. S. Sankar and A. E. Berkowitz, Phys. Rev. **B** 62, 14273 (2000)
50. S. I. Denisov, T. V. Lyutyy and K. N. Trohidou, Phys. Rev. B **67**, 014411 (2003)
51. S. Mitani, H. Fujimori, S. Ohnuma, J. Magn. Magn. Mater., 165, 141, (1997)